ChemPubSoc Europe

DOI: 10.1002/cctc.201500101

CHEMCATCHEM Full Papers

VIP

Synthesis of a Fe–Ni Alloy on a Ceria Support as a Noble-Metal-Free Catalyst for Hydrogen Production from Chemical Hydrogen Storage Materials

Kohsuke Mori,*[a, b] Tomohisa Taga,[a] and Hiromi Yamashita*[a, b]

Bimetallic FeNi nanoparticles supported on CeO_2 was proven to be effective for hydrogen production from ammonia–borane (NH_3–BH_3) as a noble-metal-free catalyst. Impregnation of iron and nickel ions with the CeO_2 surface followed by in situ reduction with $NaBH_4$ prior to catalytic dehydrogenation of AB produced highly dispersed and partially oxidized amorphous FeNi NPs stabilized by strong interaction with the CeO_2 support by Ni–O–Ce and Fe–O–Ce bonding. Investigation of the influence of the Fe/Ni ratio revealed a volcano-shaped relationship with a maximum at Fe/Ni = 1. FeNi/CeO_2 was further applicable to dehydrogenation from dimethylamine–borane ($(CH_3)_2NHBH_3$). The advantages of this catalytic system, such as the facile preparation method, free of noble metals, and high recyclability, with easy recovery from the reaction mixture by application of an external magnet, are particularly desirable for a hydrogen vector in terms of potential industrial application in fuel cells.

Introduction

Hydrogen (H_2) is an ideal clean energy carrier and is regarded as the most promising next-generation energy to replace fossil fuels.[1] However, the potential of hydrogen has not been fully utilized because of the difficulties involved in storage and transportation.[2] Thus, efficient and convenient storage of hydrogen is still one of the key issues for the hydrogen economy in the future. There has been rapidly growing interest in the search for suitable hydrogen storage materials, such as metal hydrides, sorbent materials, and chemical hydrides.[3] Among them, ammonia–borane (NH_3–BH_3, AB) has attracted much research interest as a leading molecular candidate for hydrogen storage materials because of its low molecular weight (30.87 g mol^{-1}), high theoretical hydrogen gravimetric capacity (19.6 wt%), and high stability in solid form at room temperature.[4] Such outstanding characteristics largely meet the 2015 US Department of Energy (DOE) targets for a hydrogen onboard application.[5]

The stored hydrogen in AB can be released by either pyrolysis[6] or hydrolysis routes.[3b] As pyrolysis requires considerably high temperatures and results in the release of only 6.5 wt% (1 equiv. based on AB) hydrogen, hydrolysis is considered the more promising process, producing 3 equivalents of hydrogen based on AB under mild reaction conditions in the presence of a suitable catalyst, as shown in Equation (1). Although several homogeneous and heterogeneous catalytic systems have been reported in the literature, noble metal catalysts, containing metals such as Ru, Pt, Pd, and Rh, have dominated owing to their superior catalytic properties,[5,7] which hinders large-scale energy application. In view of the strong social demand and the costliness of using noble metals, earth abundant and less expensive first-row transition metals, including Ni, Co, and Fe, have also been studied for this purpose,[8] but they require further improvements in catalytic efficiency. It is therefore believed that the development of active and durable catalysts using non-noble metals is an urgent task in the application of released hydrogen as a direct fuel source for polymer electrolyte membrane fuel cells.

$$NH_3BH_3 + 2\,H_2O \rightarrow NH_4^+ + BO_2^- + 3\,H_2 \quad (1)$$

The fabrication of bimetallic nanoparticles (NPs) has attracted much attention owing to their potential application in catalysis, which originates from the interplay of electronic and lattice effects of the neighboring metals.[9] Because of such synergistic effects, bimetallic catalysts can show significantly higher catalytic activity than their monometallic counterparts. The use of several bimetallic NPs, including Fe–Ni, Pt–Ni, and Ru–Ni, has been reported in dehydrogenation reactions of AB.[10] Although NP-based catalysts with extremely large surface areas are key components of catalytic activity, their high propensity to aggregate and difficulties with the separation step become troublesome. To overcome these drawbacks, small NPs have generally been used on suitable supports, such as polymers, metal oxides, mesostructured materials, and carbon materials, which also provide unique catalytic functions including site

[a] Prof. Dr. K. Mori, T. Taga, Prof. Dr. H. Yamashita
Division of Materials and Manufacturing Science
Graduate School of Engineering
Osaka University
2-1 Yamada-oka, Suita, Osaka 565-0871 (Japan)
Fax: (+81) 6-6879-7460
E-mail: mori@mat.eng.osaka-u.ac.jp
yamashita@mat.eng.osaka-u.ac.jp

[b] Prof. Dr. K. Mori, Prof. Dr. H. Yamashita
Elements Strategy Initiative for Catalysts Batteries ESICB
Kyoto University
Katsura, Kyoto 615-8520 (Japan)

isolation of active metal NPs, cooperative action by several sites, and synergic effects owing to the strong metal-support interactions.[9a,11]

Herein we report the in situ generation, characterization, and catalytic application of Fe–Ni nanoparticles supported on CeO_2. Iron(II) and nickel(II) ions impregnated on the surface of CeO_2 were reduced with $NaBH_4$ prior to catalytic dehydrogenation of AB. CeO_2 and $NaBH_4$ have emerged as a promising combination of support and reducing reagent to optimize catalytic activity. Investigation using a series of Fe_xNi_{1-x} bimetallic NPs deposited on CeO_2 indicated a volcano-shaped relationship with changing Fe/Ni ratios. The activity of the catalyst at a Fe/Ni ratio of 1 was proven to be superior to that of a previously reported colloidal FeNi alloy catalyst and FeNi/SBA-15, which may be attributed to the strong interactions between FeNi NPs and the CeO_2 support. As well as this, a synergic alloying effect plays a crucial role in achieving high catalytic activity. Furthermore, the catalytic system studied in this work provides an opportunity for convenient separation after the catalytic reaction by application of an external magnet, and the recovered catalyst can be reused without any loss of activity.

Results and Discussion

The deposition of both Fe and Ni on the surface of CeO_2 was performed by a simple impregnation method from an aqueous solution of $FeSO_4{\cdot}7H_2O$ and $NiCl_2{\cdot}6H_2O$. The FeNi NPs were synthesized in situ by reduction with $NaBH_4$ and then employed in the catalytic dehydrogenation of AB. Several FeNi catalysts were also prepared by the same method using various inorganic supports.

Initially, the dehydrogenation of AB was performed using various FeNi catalysts. The results are summarized in Figure 1, together with the BET surface area of the supports, determined by the N_2 adsorption–desorption. No induction period was observed, and H_2 was stoichiometrically produced in a 3:1 (H_2/NH_3BH_3) molar ratio during the course of the reaction for all samples, indicating the occurrence of complete dehydrogenation. FeNi/CeO_2 exhibited the highest activity among the investigated catalysts, and FeNi/ZrO_2 and FeNi/MgO showed substantially low catalytic activity. There was no significant relationship between catalytic activity and BET surface area. The BET surface area of CeO_2 is 120 $m^3 g^{-1}$ nm, which is moderate compared to that of other supports. However, amorphous SiO_2 and mesoporous silica SBA-15 showed low activity despite of their relatively large surface areas, whereas Al_2O_3 showed moderate activity despite its relatively small surface area. During the reduction sequence with $NaBH_4$, the color of the catalyst turned black immediately for all samples except FeNi/MgO. The color of FeNi/MgO after reduction remained pale yellow, suggesting that the stability of Fe and Ni ions on the surface of MgO toward reduction is the main reason for its low activity. Additionally, the catalytic activity of the FeNi/CeO_2 was also greatly influenced by the reducing reagent: $NaBH_4$ reduction is the best method for attaining high catalytic activity, as shown in Figure 2. The use of HCOONa or AB, the reduction abilities

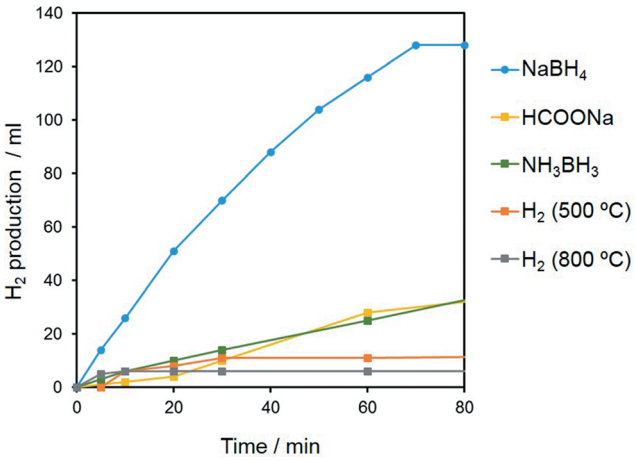

Figure 2. Effect of reducing reagent of the FeNi/CeO_2 in the hydrogen production from AB.

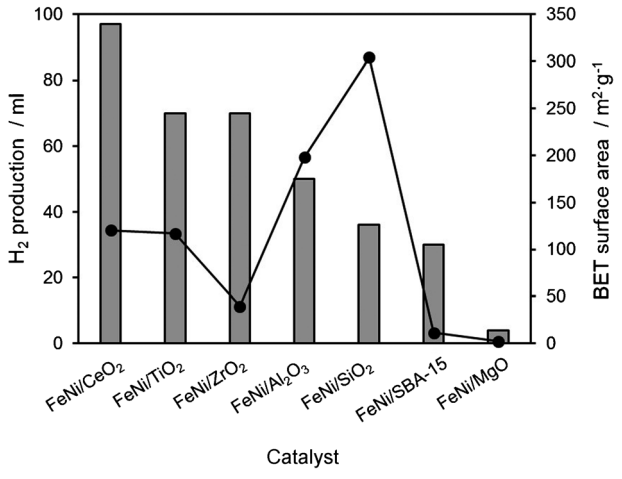

Figure 1. Hydrogen production from AB and BET surface area of various catalysts.

of which are relatively low, resulted in moderate activity, whereas H_2 reduction gave poor results regardless of the temperature. In the preliminary experiment, the calcined sample at 674 K before $NaBH_4$ reduction showed almost no activity. Accordingly, it was speculated that the local structure of the FeNi nanoparticles rather than the surface area of the support might be an important factor in achieving high catalytic activity. This was supported by structural characterization, as will be discussed later.

The composition of the FeNi/CeO_2 samples (Fe/Ni = 1:0, 2:1, 1:1, 1:2, 1:3, and 0:1) was easily adjusted by varying the initial molar ratio of $FeSO_4{\cdot}7H_2O$ and $NiCl_2{\cdot}6H_2O$ in the impregnation sequence. The time course for hydrogen production from AB using various FeNi/CeO_2 combinations with different compositions is shown in Figure 3, and the inset shows a plot of turnover number (TON) versus the mole fraction of Ni at different compositions. The reactions using pure Fe/CeO_2 and Ni/CeO_2 were seriously sluggish, but an enhancement effect was ob-

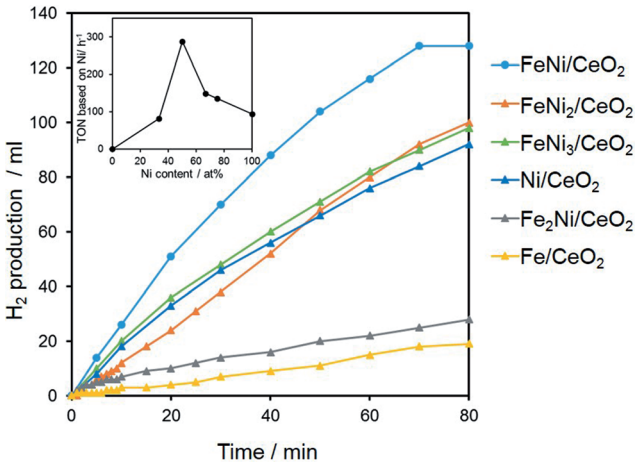

Figure 3. Effect of Fe/Ni molar ratio in the hydrogen production from AB. Inset shows the TON versus Ni content.

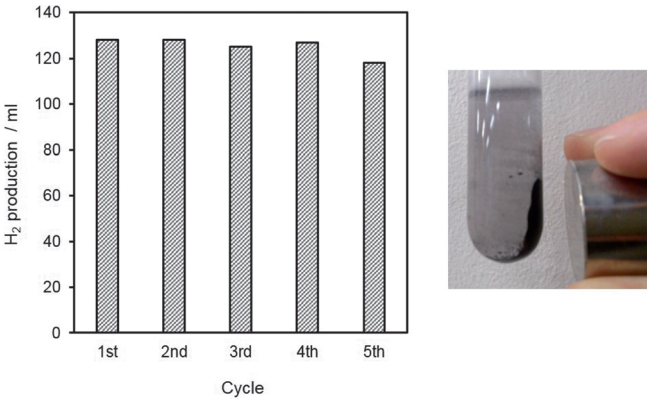

Figure 4. Recycling results for hydrogen production from AB and the photograph of the separation of $FeNi/CeO_2$ from reaction mixture using an external magnet.

served when Fe and Ni were alloyed. This result indicates that a synergic effect exists between Fe and Ni atoms. The maximum activity was obtained at a ratio of Fe/Ni = 1:1. Such a volcano-shaped activity order clearly suggests that the formation of a uniform FeNi alloy structure on the surface of CeO_2 and the synergic effect originated from the integration of Fe with Ni.

The activation energy (E_a) for the dehydrogenation of AB using $FeNi/CeO_2$, determined by Arrhenius plots, was 54.3 kJ mol^{-1}. This value is lower than those obtained for the reaction using unsupported colloidal FeNi (114.0 kJ g^{-1}),[10a] FeNi/SBA-15 (75.0 kJ mol^{-1}),[10a] and Ni powder (70.0 kJ mol^{-1}),[12] suggesting that the positive effect of the CeO_2 support is not only the achievement of easy separation from the reaction mixture but also an enhancement in the catalytic activity. Furthermore, the TON of $FeNi/CeO_2$, based on Ni atoms, approached 288 h^{-1}. Notably, the TON achieved by $FeNi/CeO_2$ was higher than those reported for other similar active catalyst systems, such as MOF-based Ni NPs (120 h^{-1}),[8d] in situ generated colloidal Fe NPs (64 h^{-1}),[8c] $Ni/\gamma\text{-}Al_2O_3$ (51 h^{-1}),[7d] and Ni hollow spheres (20 h^{-1}).[12]

A more important advantage of the $FeNi/CeO_2$ is its facile recovery from the reaction mixture and high reusability (Figure 4). FeNi NPs are expected to be a single magnetic domain and exhibit a magnetic moment only in the presence of a magnetic field, indicating a superparamagnetic nature; the particles immediately return to their nonmagnetic state if the magnetic field is removed.[13] Upon completion of the reaction, the magnetic properties of the $FeNi/CeO_2$ afford a straightforward means of isolating the catalyst from the reaction mixture. An external permanent magnet attracted the catalyst, and the recovered catalyst could then be recycled in the dehydrogenation of AB at least five times while maintaining an inherent activity that was identical to the initial run. It can be concluded that the present catalytic system suppresses the negative effect of the accumulated BO_2^- ions to the minimum.

The $FeNi/CeO_2$ catalytic system was further applied to dehydrogenation of dimethylamine–borane ($(CH_3)_2NHBH_3$; DMAB), which is also identified as one of the most promising candidates for a chemical hydrogen storage material because of its high gravimetric hydrogen content (7.4%), high stability, and low cost compared to AB.[4a] Many catalytic systems have been reported previously, but most research has been focused on homogeneous catalytic systems based on the precious metals Ru, Ir, and Rh.[14] To date, the employment of heterogeneous systems, such as Pd/carbon[14b] and skeletal Ni catalysts,[15] has been limited to a few reports.

As summarized in Figure 5, dehydrogenation of DMAB was performed by using various FeNi catalysts. Hydrogen evolution

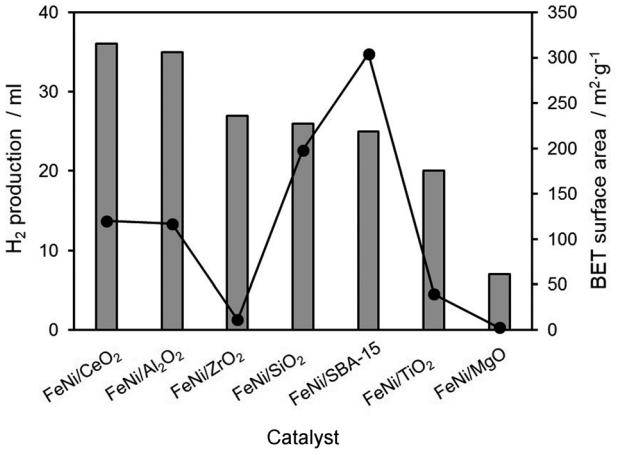

Figure 5. Hydrogen production from DMAB and BET surface area of various catalysts.

occurred until one equivalent of H_2 per mol of DMAB is liberated, indicating that the reaction proceeds according to Equation (2). The catalytic tendency was similar to that for dehydrogenation of AB; $FeNi/CeO_2$ and $FeNi/Al_2O_3$ exhibited the highest activity, whereas $FeNi/ZrO_2$, $FeNi/SiO_2$, and $FeNi/TiO_2$ gave moderate results. Again, FeNi/MgO showed substantially lower catalytic activity because of the high resistance of Fe and Ni ions toward reduction on MgO. In Figure 5, the BET surface

areas of the supports are also included. There was no significant relationship between catalytic activity and BET surface area, as was the case for AB dehydrogenation.

$$2Me_2NHBH_3 \longrightarrow \begin{matrix} Me_2N{-}BH_2 \\ | \quad | \\ H_2B{-}NMe_2 \end{matrix} + 2H_2 \qquad (2)$$

As mentioned before, the local structure of the FeNi nanoparticles generated in situ on the respective supports may play a crucial role in attaining high catalytic activity. To elucidate the structure–activity relationship in the dehydrogenation of AB, characterization of the active FeNi/CeO_2 and the less active FeNi/ZrO_2 was performed for comparison purposes. In the XRD pattern, the intensities of diffraction peaks were low for both samples, presumably as a result of the smaller size of the particles. The contrast of the FeNi NPs in the TEM image is obscure, and it is difficult to distinguish FeNi NPs in FeNi/CeO_2, because the CeO_2 support may prevent the transmission of electrons. Thus, a scanning transmission electron microscopy (STEM) image with elemental mapping was obtained. As depicted in Figure 6, elemental mapping of FeNi/CeO_2 demonstrated that

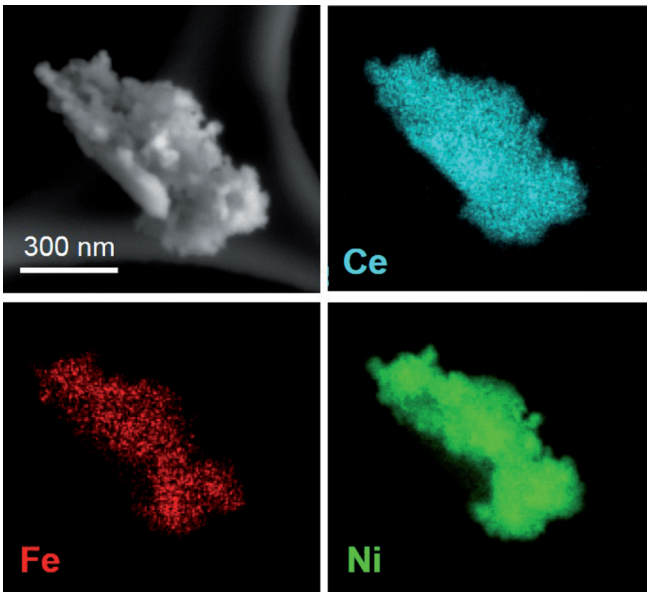

Figure 6. FESEM image and elemental mapping of FeNi/CeO_2.

both Fe and Ni species were highly dispersed throughout the image area, indicating the formation of a uniform FeNi alloy structure on the surface of CeO_2. On the ZrO_2 support, however, Fe and Ni atoms were partially segregated on the surface (Figure 7). This means that not only FeNi alloy NPs but also monometallic Fe or Ni NPs were generated in the case of FeNi/ZrO_2. The difference in the dispersity of Fe and Ni atoms on each support may be ascribed to the reducibility of each ion. In the H_2 TPR measurements of the as-synthesized samples, FeNi/CeO_2 displayed a bimodal reduction peak at approximately 385 and 470 °C, which was attributed to the reduction of

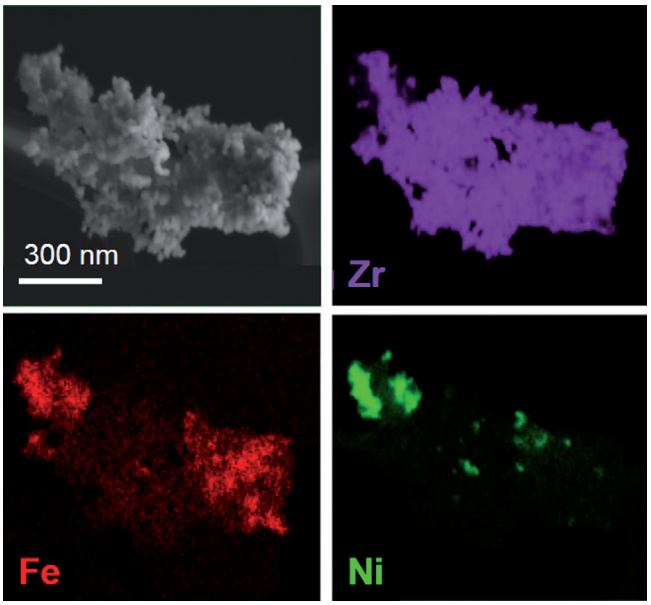

Figure 7. FESEM image and elemental mapping of FeNi/ZrO_2.

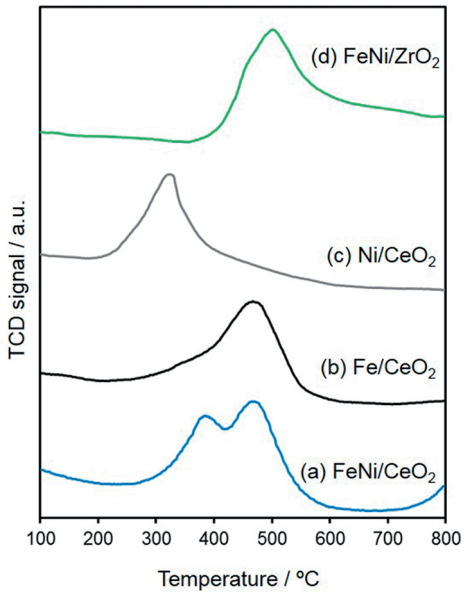

Figure 8. H_2 TPR profiles of a) FeNi/CeO_2, b) Fe/CeO_2, c) Ni/CeO_2, and d) FeNi/ZrO_2.

Ni^{2+} and Fe^{2+}, respectively (Figure 8a). In contrast, one broad reduction profile centered at 510 °C, with a shoulder peak at a lower temperature, was observed in the case of FeNi/ZrO_2 (Figure 8d). This result suggests that the CeO_2 support allows rapid reduction of Fe and Ni ions rather than ZrO_2. It is well accepted that the kinetics of the reduction of metal ions play a crucial role in determining the final particle size; rapid reduction generates more metal nuclei in a shorter period and efficiently suppresses the growth of metal NPs.[16] Therefore, CeO_2 supports may produce smaller FeNi NPs than ZrO_2.

X-ray absorption measurements were performed to investigate the local structure and chemical environment of FeNi/

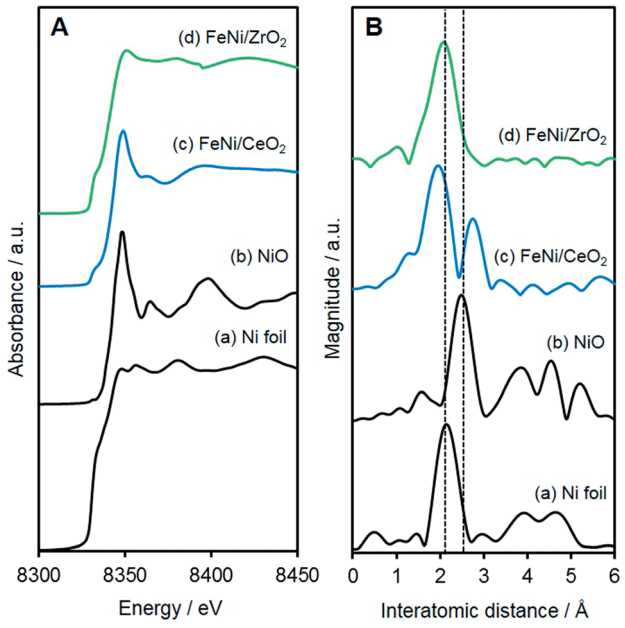

Figure 9. A) Ni K-edge XANES spectra and B) FT EXAFS spectra of a) Ni foil, b) NiO, c) $NiFe_2O_4$, d) $FeNi/CeO_2$ reduced with $NaBH_4$, e) $FeNi/ZrO_2$ reduced with $NaBH_4$, and f) $FeNi/CeO_2$ reduced with H_2 at 773 K.

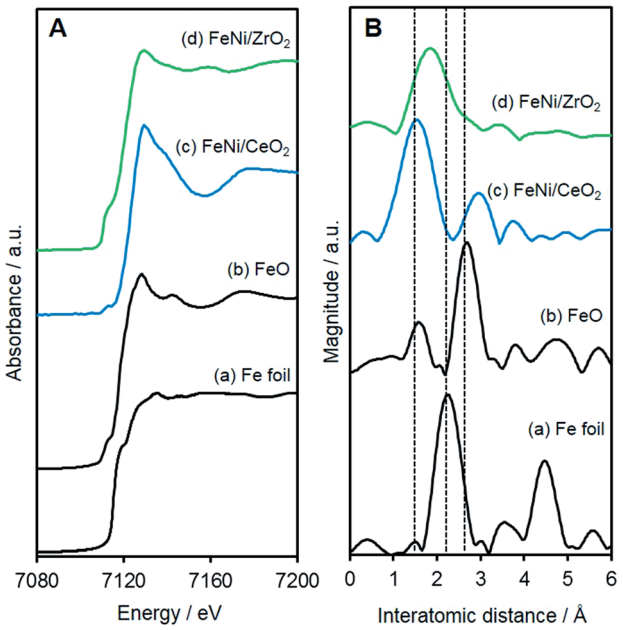

Figure 10. A) Fe K-edge XANES spectra and B) FT EXAFS spectra of a) Fe foil, b) FeO, c) $NiFe_2O_4$, d) $FeNi/CeO_2$ reduced with $NaBH_4$, e) $FeNi/ZrO_2$ reduced with $NaBH_4$, and f) $FeNi/CeO_2$ reduced with H_2 at 773 K.

CeO_2 in comparison with $FeNi/ZrO_2$. In Figure 9A normalized X-ray absorption near-edge structure (XANES) spectra at the Ni K-edge of FeNi supported catalysts are shown as well as those of standard samples including Ni foil, NiO, and $NiFe_2O_4$. $FeNi/CeO_2$, NiO, and $NiFe_2O_4$ exhibited a distinct white-line absorption peak at 8348 eV with higher intensity. More detailed inspection revealed that the white-line absorption peak of $FeNi/CeO_2$ was lower than those for NiO and $NiFe_2O_4$, indicating that the Ni atoms of $FeNi/CeO_2$ exist in a lower oxidation state than those of NiO and $NiFe_2O_4$. In contrast, $FeNi/ZrO_2$ and Ni foil afforded lower intensified peaks at 8348 eV, suggesting that the oxidation state of Ni remained Ni^0.

In Figure 9B, the Fourier transforms (FT) of Ni K-edge extended X-ray absorption fine structure (EXAFS) spectra of these samples are shown. Both $FeNi/CeO_2$ and $FeNi/ZrO_2$ samples exhibited a main peak at approximately 2.0 Å, which could be assigned to the contiguous Ni–Ni bond in the metallic form. The Ni–Ni distance in $FeNi/CeO_2$, however, was found to be slightly shorter than those of pure Ni metal and $FeNi/ZrO_2$, suggesting the presence of Fe–Ni heteroatomic bonding in $FeNi/CeO_2$. $FeNi/CeO_2$ also exhibited another peak at 2.85 Å in the second coordination region, which may be mainly attributed to Ni–O–Ce bonds, because the position of this second peak differs from those of Ni–O–Ni and Ni–O–Fe observed in NiO and $NiFe_2O_4$, respectively.

In Figure 10A the Fe K-edge XANES spectra of the FeNi catalysts and reference iron compounds are shown. The edge position (measured at the half-height of the edge jump) depends on the electronic charge of the iron ion, and the energy increased in the following order: Fe foil (7115.9 eV) < $FeNi/ZrO_2$ (7119.2 eV) < $FeNi/CeO_2$ (7121.9 eV) < FeO (7122.0 eV) < $NiFe_2O_4$ (7123.7 eV). Thus, the iron elements in the FeNi samples are a mixture of Fe^0 and Fe^{2+}, suggesting that the Fe atoms in $FeNi/CeO_2$ exist in a more oxidized state than those in $FeNi/ZrO_2$.

The FT EXAFS spectra of $FeNi/CeO_2$ displayed a main peak corresponding to Fe–O at 1.5 Å, accompanied by a slight peak at approximately 3.0 Å. Compared to the Fe–O–Fe bond of FeO, the position of the second peak was shifted slightly to a longer interatomic distance, which was partially similar to that of the Fe–O–Ni bond observed in $NiFe_2O_4$. Thus, this peak may be attributed to contiguous Fe–O–Ni as well as Fe–O–Ce bonds by strong interaction with the CeO_2 support (Figure 10B). The insertion of metals into the surface CeO_2 lattice as a result of a strong metal–support interaction has been reported in noble-metal/CeO_2 systems, which would lead to a high degree of dispersion of metals with high stability.[17] For the structural model of the $FeNi/CeO_2$, the overall results suggest the formation of partially oxidized amorphous FeNi NPs with a small size, which are stabilized by a strong interaction with CeO_2 by Ni–O–Ce and Fe–O–Ce bonding. In contrast, $FeNi/ZrO_2$ exhibited a main peak at approximately 2.0 Å, which was slightly different from the peaks for both the Fe–O and the Fe–Fe bonds, indicating the presence of structurally disordered FeO and FeNi phases. Upon consideration of the H_2 TPR results (Figure 8) as well as the reduction potentials of ions ($E^0(Ni^{2+}/Ni^0) = -0.257$ V, $E^0(Fe^{2+}/Fe^0) = -0.44$ V vs. normal hydrogen electrode), the structural model of $FeNi/ZrO_2$ allows the reasonable supposition that most of the Ni atoms are preferentially located in the core region, whereas the Fe atoms are preferentially located in the shell region. Thus, the Fe atoms are more oxidized than the Ni atoms because of their exposure to the surface.

Plotting H_2 generation rate versus metal concentration, both on logarithmic scales, gives a straight line with a slope of 1.04.

Thus an apparent first-order dependence on catalyst concentration was observed. This observation indicates that the hydrogen generation rate is controlled by the surface reaction. Thus the increased active sites on small NPs are expected to exhibit high catalytic activity in the dehydrogenation of AB. It has been reported that a possible mechanism for catalytic dehydrogenation of AB involves the following three steps: i) formation of an activated complex species between AB and the metal particle surface, ii) concerted dissociation of the B–N bond upon attack by a H_2O molecule, and iii) hydrolysis of the resulting BH_3 intermediate to produce H_2 along with the formation of a BO_2^- ion.[18] The superior catalytic activity of FeNi/CeO_2 may be attributed to the formation of highly dispersed FeNi NPs as well as structurally distorted Ni–O–Ce and Fe–O–Ce bonding. Such amorphous FeNi catalysts provide a much higher concentration of surface active sites to promote the formation of an activated complex, which is most likely the rate-determining step. In homogeneous catalysis using metal halides, the addition of a Lewis acid such as Co^{2+} ions to the reaction mixture enhanced H_2 production activity, which can be simply explained by cooperative activation of Lewis-basic AB with the assistance of the electron-deficient Lewis-acidic Co^{2+} ions.[19] Thus, we predict that the neighboring Lewis-acidic Ce sites (Ni–O–Ce and Fe–O–Ce) also have a positive effect on the enhancement of catalytic activity.

The effect of a reducing reagent in the preparation of FeNi NPs on the catalytic activity was also evidenced by the XAFS analysis. The Ni K-edge XANES and FT EXAFS spectra of FeNi/CeO_2 prepared by reduction with molecular hydrogen at 773 K are similar to those of Ni foil but differ from those of NiO and $NiFe_2O_4$ (Figure 9). Fe K-edge XAFS spectra also confirm the formation of Fe–Ni bonds in the metallic form (Figure 10). Such an observation in H_2-treated FeNi/CeO_2 is consistent with the results of $NaBH_4$-treated FeNi/ZrO_2, as described earlier, verifying the crystalline nature of the particles. Thus, we conclude that the amorphous character is essential to attain high activity of FeNi NPs in the dehydrogenation of AB, because of the exposure of active Ni–O–Ce and Fe–O–Ce sites for the catalytic reaction compared to its crystalline counterparts. Similar phenomena have been reported for Fe NP-catalyzed dehydrogenation of AB, in which in situ synthesized amorphous Fe NPs composed of zero-valent Fe showed unexpectedly higher activity in the hydrogenation of AB than as-synthesized α-Fe crystallites.[8c]

Conclusions

The synthesis and characterization of FeNi/CeO_2 and an evaluation of its catalytic activity in the catalytic dehydrogenation of ammonia–borane (NH_3–BH_3) are presented. The impregnated iron(II) and nickel(II) ions on CeO_2 were reduced with $NaBH_4$ prior to catalytic dehydrogenation of ammonia–borane. CeO_2 was proven to be an appropriate catalyst support to optimize catalytic activity. Characterization by several physicochemical methods revealed that the highly dispersed FeNi NPs were stabilized on the surface of CeO_2 by strong interactions. In contrast, FeNi/ZrO_2, which exhibited inferior activity to FeNi/CeO_2, showed partially segregated Fe and Ni atoms on its surface. An investigation using a series of FeNi/CeO_2 combinations with different Fe/Ni ratios resulted in a volcano-shaped relationship. The catalytic system described here is a powerful candidate for a H_2 generation protocol, thanks to the following advantages: (i) no requirement of noble metals, (ii) simple work-up procedures by application of an external magnet and the durability of catalyst lifetime, (iii) superior catalytic activity to colloidal FeNi or FeNi/SBA-15, and iv) applicability to dehydrogenation from dimethylamine–borane ($(CH_3)_2NHBH_3$).

Experimental Section

Materials

CeO_2 (JRC-CEO-1) was supplied from the Japan Catalysis Society. $FeSO_4{\cdot}7H_2O$, $NiCl_2{\cdot}6H_2O$, and ZrO_2 were purchased from Nacalai Tesque. Ammonia borane (NH_3–BH_3, AB) and dimethylamine–borane ($(CH_3)_2NHBH_3$; DMAB) were obtained from Aldrich Chemical Co. All commercially available compounds were used as received. The ordinary distilled water was used as reaction solvent.

Preparation of catalyst

CeO_2 (0.5 g) was mixed with a 100 mL volume of aqueous solution containing $FeSO_4{\cdot}7H_2O$ (0.05 g, 0.18 mmol), $NiCl_2{\cdot}6H_2O$ (0.043 g, 0.18 mmol) and stirred at room temperature for 1 h. The suspension was evaporated under vacuum, and the obtained powder was dried overnight, giving FeNi/CeO_2. In this way, the FeNi/CeO_2 samples with different Fe/Ni ratios (Fe:Ni = 1:0, 2:1, 1:1, 1:2, 1:3, and 0:1) were prepared. FeNi/TiO_2, FeNi/ZrO_2, FeNi/Al_2O_3, FeNi/SiO_2, FeNi/SBA-15, and FeNi/MgO were also synthesized according to this procedure.

Catalytic study using in situ synthesized FeNi alloy catalyst

In a typical experiment, the FeNi/CeO_2 catalyst (0.02 g) was placed into a Schlenk-type reaction vessel (30 mL) connected with gas burette. After the purging with Ar for three times, a 10 mL volume of aqueous solution of $NaBH_4$ (0.015 mmol) was added and gently stirred for 1 h. The evolution of gas was monitored by using a gas burette. After the reduction was completed, a 1 mL volume of aqueous solution of AB (1.92 mmol) was further added into the reaction vessel and reacted at 303 K to study the catalytic activity of the as-synthesized catalyst. The reaction was started when the AB solution was added to the reaction vessel.

Characterization

Powder X-ray diffraction patterns were recorded by using a Rigaku Ultima IV diffractometer with $Cu_{K\alpha}$ radiation ($\lambda = 1.5406$ Å). BET surface area measurements were performed by using a BEL–SORP max (Bel Japan, Inc.) instrument at 77 K. The sample was degassed in vacuum at 353 K for 24 h prior to data collection. Inductively coupled plasma optical emission spectrometry measurements were performed using a Nippon Jarrell-Ash ICAP-575 Mark II instrument. SEM–EDX measurement was performed by HITACHI SU8220 FESEM equipped with XFLASH5060FQ detector. Fe K-edge and Ni K-edge XAFS spectra were recorded at RT in fluorescence mode at the BL-9A facility at the Photon Factory in the National Laboratory for High-Energy Physics, Tsukuba (2012G126). A Si(111) double crystal

was used to monochromatize the X-rays from the 2.5 GeV electron storage ring. In a typical experiment, the sample was loaded into the in situ cell with plastic windows. The EXAFS data were examined by using an EXAFS analysis program, Rigaku EXAFS. Fourier transformation of k^3-weighted normalized EXAFS data was performed over the 3.0 Å $< k/$Å$^{-1} <$ 12 Å range to obtain the radial structure function.

Acknowledgements

The present work was partially supported by MEXT program "Elements Strategy Initiative to Form Core Research Center", MEXT; Ministry of Education Culture, Sports, Science, and Technology, Japan. We acknowledge Hitachi High-Technologies Corporation for their assistance with the SEM-EDX measurements (HITACHI SU8220 FESEM & XFLASH5060FQ). XAFS spectra were recorded at the BL-9A facilities of the Photon Factory at the National Laboratory for High-Energy Physics, Tsukuba (2012G126).

Keywords: boranes · cerium · dehydrogenation · iron · nickel

[1] a) B. C. H. Steele, A. Heinzel, *Nature* **2001**, *414*, 345 – 352; b) U. Eberle, M. Felderhoff, F. Schüth, *Angew. Chem. Int. Ed.* **2009**, *48*, 6608 – 6630; *Angew. Chem.* **2009**, *121*, 6732 – 6757.

[2] a) J. Yang, A. Sudik, C. Wolverton, D. J. Siegel, *Chem. Soc. Rev.* **2010**, *39*, 656 – 675; b) A. W. C. van den Berg, C. O. Arean, *Chem. Commun.* **2008**, 668 – 681.

[3] a) H.-L. Jiang, S. K. Singh, J.-M. Yan, X.-B. Zhang, Q. Xu, *ChemSusChem* **2010**, *3*, 541 – 549; b) M. Yadav, Q. Xu, *Energy Environ. Sci.* **2012**, *5*, 9698 – 9725; c) S.-i. Orimo, Y. Nakamori, J. R. Eliseo, A. Züttel, C. M. Jensen, *Chem. Rev.* **2007**, *107*, 4111 – 4132.

[4] a) A. Staubitz, A. P. M. Robertson, I. Manners, *Chem. Rev.* **2010**, *110*, 4079 – 4124; b) T. B. Marder, *Angew. Chem. Int. Ed.* **2007**, *46*, 8116 – 8118; *Angew. Chem.* **2007**, *119*, 8262 – 8264.

[5] E. K. Abo-Hamed, T. Pennycook, Y. Vaynzof, C. Toprakcioglu, A. Koutsioubas, O. A. Scherman, *Small* **2014**, *10*, 3145 – 3152.

[6] A. Gutowska, L. Li, Y. Shin, C. M. Wang, X. S. Li, J. C. Linehan, R. S. Smith, B. D. Kay, B. Schmid, W. Shaw, M. Gutowski, T. Autrey, *Angew. Chem. Int. Ed.* **2005**, *44*, 3578 – 3582; *Angew. Chem.* **2005**, *117*, 3644 – 3648.

[7] a) S. Akbayrak, S. Ozkar, *Dalton Trans.* **2014**, *43*, 1797 – 1805; b) N. Cao, T. Liu, J. Su, X. Wu, W. Luo, G. Cheng, *New J. Chem.* **2014**, *38*, 4032 – 4035; c) X. Wang, D. Liu, S. Song, H. Zhang, *Chem. Eur. J.* **2013**, *19*, 8082 – 8086; d) M. Chandra, Q. Xu, *J. Power Sources* **2007**, *168*, 135 – 142; e) X. Qian, Y. Kuwahara, K. Mori, H. Yamashita, *Chem. Eur. J.* **2014**, *20*, 15746 – 15752; f) H. Cheng, T. Kamegawa, K. Mori, H. Yamashita, *Angew. Chem. Int. Ed.* **2014**, *53*, 2910 – 2914; *Angew. Chem.* **2014**, *126*, 2954 – 2958; g) K. Fuku, R. Hayashi, S. Takakura, T. Kamegawa, K. Mori, H. Yamashita, *Angew. Chem. Int. Ed.* **2013**, *52*, 7446 – 7450; *Angew. Chem.* **2013**, *125*, 7594 – 7598.

[8] a) -C. Luo, Y.-H. Liu, Y. Hung, X.-Y. Liu, C.-Y. Mou, *Int. J. Hydrogen Energy* **2013**, *38*, 7280 – 7290; b) X. Shan, J. Du, F. Cheng, J. Liang, Z. Tao, J. Chen, *Int. J. Hydrogen Energy* **2014**, *39*, 6987 – 6994; c) J.-M. Yan, X.-B. Zhang, S. Han, H. Shioyama, Q. Xu, *Angew. Chem. Int. Ed.* **2008**, *47*, 2287 – 2289; *Angew. Chem.* **2008**, *120*, 2319 – 2321; d) Y. Li, L. Xie, Y. Li, J. Zheng, X. Li, *Chem. Eur. J.* **2009**, *15*, 8951 – 8954; e) Ö. Metin, V. Mazumder, S. Özkar, S. Sun, *J. Am. Chem. Soc.* **2010**, *132*, 1468 – 1469; f) J. F. Sonnenberg, R. H. Morris, *ACS Catal.* **2013**, *3*, 1092 – 1102.

[9] a) K. Mori, H. Yamashita, *Phys. Chem. Chem. Phys.* **2010**, *12*, 14420 – 14432; b) R. Ferrando, J. Jellinek, R. L. Johnston, *Chem. Rev.* **2008**, *108*, 845 – 910; c) R. Ghosh Chaudhuri, S. Paria, *Chem. Rev.* **2012**, *112*, 2373 – 2433; d) K. Fuku, T. Sakano, T. Kamegawa, K. Mori, H. Yamashita, *J. Mater. Chem.* **2012**, *22*, 16243 – 16247.

[10] a) S.-W. Lai, H.-L. Lin, Y.-P. Lin, T. L. Yu, *Int. J. Hydrogen Energy* **2013**, *38*, 4636 – 4647; b) J.-M. Yan, X.-B. Zhang, S. Han, H. Shioyama, Q. Xu, *J. Power Sources* **2009**, *194*, 478 – 481; c) K. Aranishi, A. K. Singh, Q. Xu, *ChemCatChem* **2013**, *5*, 2248 – 2252; d) S. Wang, D. Zhang, Y. Ma, H. Zhang, J. Gao, Y. Nie, X. Sun, *ACS Appl. Mater. Interfaces* **2014**, *6*, 12429 – 12435; e) G. Chen, S. Desinan, R. Rosei, F. Rosei, D. Ma, *Chem. Eur. J.* **2012**, *18*, 7925 – 7930.

[11] K. Mori, H. Yamashita, *J. Jpn. Pet. Inst.* **2011**, *54*, 1 – 14.

[12] F. Cheng, H. Ma, Y. Li, J. Chen, *Inorg. Chem.* **2007**, *46*, 788 – 794.

[13] a) K. Mori, Y. Kondo, H. Yamashita, *Phys. Chem. Chem. Phys.* **2009**, *11*, 8949 – 8954; b) K. Mori, N. Yoshioka, Y. Kondo, T. Takeuchi, H. Yamashita, *Green Chem.* **2009**, *11*, 1337 – 1342.

[14] a) M. Gulcan, M. Zahmakiran, S. Özkar, *Appl. Catal. B* **2014**, *147*, 394 – 401; b) C. A. Jaska, K. Temple, A. J. Lough, I. Manners, *J. Am. Chem. Soc.* **2003**, *125*, 9424 – 9434.

[15] A. P. M. Robertson, R. Suter, L. Chabanne, G. R. Whittell, I. Manners, *Inorg. Chem.* **2011**, *50*, 12680 – 12691.

[16] K. Mori, T. Hara, T. Mizugaki, K. Ebitani, K. Kaneda, *J. Am. Chem. Soc.* **2004**, *126*, 10657 – 10666.

[17] S. Colussi, A. Gayen, M. Farnesi Camellone, M. Boaro, J. Llorca, S. Fabris, A. Trovarelli, *Angew. Chem. Int. Ed.* **2009**, *48*, 8481 – 8484; *Angew. Chem.* **2009**, *121*, 8633 – 8636.

[18] a) Q. Xu, M. Chandra, *J. Power Sources* **2006**, *163*, 364 – 370; b) M. Mahyari, A. Shaabani, *J. Mater. Chem. A* **2014**, *2*, 16652 – 16659.

[19] R. Chiriac, F. Toche, U. B. Demirci, O. Krol, P. Miele, *Int. J. Hydrogen Energy* **2011**, *36*, 12955 – 12964.

Received: February 2, 2015
Published online on April 9, 2015